6-19-2020

Development of a single-stranded DNA-binding protein fluorescent fusion toolbox

Katarzyna Dubiel
University of Wisconsin School of Medicine and Public Health

Camille Henry
University of Wisconsin, Madison

Lisanne M. Spenkelink
University of Wollongong

Alexander G. Kozlov
Washington University School of Medicine in St. Louis

Elizabeth A. Wood
University of Wisconsin, Madison

See next page for additional authors

Published online 6 May 2020

Nucleic Acids Research, 2020, Vol. 48, No. 11 ***6053–6067***
doi: 10.1093/nar/gkaa320

Development of a single-stranded DNA-binding protein fluorescent fusion toolbox

Katarzyna Dubiel[1], Camille Henry[2], Lisanne M. Spenkelink[3,4], Alexander G. Kozlov[5], Elizabeth A. Wood[2], Slobodan Jergic[3,4], Nicholas E. Dixon[3,4], Antoine M. van Oijen[3,4], Michael M. Cox[2], Timothy M. Lohman[5], Steven J. Sandler[6] and James L. Keck[1,*]

[1]Department of Biomolecular Chemistry, University of Wisconsin School of Medicine and Public Health, Madison, WI 53706, USA, [2]Department of Biochemistry, University of Wisconsin - Madison, Madison, WI 53706, USA, [3]Molecular Horizons and School of Chemistry and Molecular Bioscience, University of Wollongong, Wollongong, New South Wales 2522, Australia, [4]Illawarra Health and Medical Research Institute, Wollongong, New South Wales 2522, Australia, [5]Department of Biochemistry and Molecular Biophysics, Washington University School of Medicine, St. Louis, MO 63110, USA and [6]Department of Microbiology, University of Massachusetts at Amherst, Amherst, MA 01003, USA

Received October 18, 2019; Revised April 15, 2020; Editorial Decision April 17, 2020; Accepted May 04, 2020

ABSTRACT

Bacterial single-stranded DNA-binding proteins (SSBs) bind single-stranded DNA and help to recruit heterologous proteins to their sites of action. SSBs perform these essential functions through a modular structural architecture: the N-terminal domain comprises a DNA binding/tetramerization element whereas the C-terminus forms an intrinsically disordered linker (IDL) capped by a protein-interacting SSB-Ct motif. Here we examine the activities of SSB-IDL fusion proteins in which fluorescent domains are inserted within the IDL of *Escherichia coli* SSB. The SSB-IDL fusions maintain DNA and protein binding activities *in vitro*, although cooperative DNA binding is impaired. In contrast, an SSB variant with a fluorescent protein attached directly to the C-terminus that is similar to fusions used in previous studies displayed dysfunctional protein interaction activity. The SSB-IDL fusions are readily visualized in single-molecule DNA replication reactions. *Escherichia coli* strains in which wildtype SSB is replaced by SSB-IDL fusions are viable and display normal growth rates and fitness. The SSB-IDL fusions form detectible SSB foci in cells with frequencies mirroring previously examined fluorescent DNA replication fusion proteins. Cells expressing SSB-IDL fusions are sensitized to some DNA damaging agents. The results highlight the utility of SSB-IDL fusions for biochemical and cellular studies of genome maintenance reactions.

INTRODUCTION

Single-stranded (ss) DNA-binding proteins (SSBs) perform critical functions in genome maintenance by binding and protecting ssDNA and by interacting with several proteins involved in DNA replication, recombination and repair (1–5). SSB binding to ssDNA prevents formation of secondary structures that can block genome maintenance processes and protects ssDNA from degradation. SSB-protein interactions function to recruit genome maintenance proteins to their sites of action and, in some instances, to stimulate the activity of partner proteins (1,6–15). While SSB functions have been investigated extensively *in vitro,* tools to probe SSB's roles *in vivo* are more limited.

Bacterial SSBs function as homotetramers and are comprised of functional N- and C-terminal elements that are bridged by an intrinsically disordered linker (IDL) (Figure 1). The N-terminus of each monomer contains an oligosaccharide/oligonucleotide-binding (OB) domain that is responsible for DNA binding and tetramerization, whereas the C-terminal-most region forms a highly-conserved protein-interaction motif referred to as the 'SSB-Ct' (4,16,17). The SSB IDL is a poorly structured region with limited sequence complexity, and all current SSB crystal structures lack electron density for this region of the protein (18–26). The length and amino acid composition of the IDL influence DNA-binding and cooperativity of *Escherichia coli* SSB (EcSSB) (27–30). Interestingly, a variant that removes the IDL (residues 113–168) of EcSSB but that leaves the SSB-Ct intact complements deletion of the *ssb* gene from *E. coli* (16). Across bacterial species, SSB IDLs have both poor conservation and variable lengths ranging from 25 to 135 residues (Supplementary Figure S1) (28,29).

To date, cellular localization studies using SSB fluorescent fusion proteins in bacteria have relied on direct C-

*To whom correspondence should be addressed. Tel: +1 608 263 1815; Email: jlkeck@wisc.edu

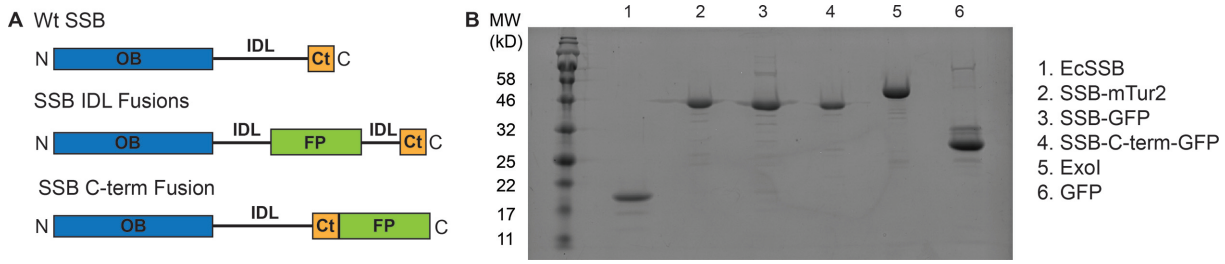

Figure 1. (**A**) Schematic of EcSSB and SSB fusions with the OB domain (blue), SSB-Ct (orange), IDL and fluorescent protein (FP, green) depicted. (**B**) SDS-PAGE gel of purified proteins.

terminal fluorescent fusions. This arrangement is likely to disrupt SSB protein interactions and experiments that use these fusions appear to require a second wild type copy of the *ssb* gene for cell viability (31–34). Other SSB fusions that rely on fluorescent labeling of Cys residues in SSB have proven to be useful *in vitro* but cannot be used in cells (35–37). Here we describe an SSB fluorescent protein fusion design in which fluorescent proteins (super-folder (sf) green fluorescent protein (GFP) or mTurquiose2 (mTur2)) are inserted within the IDL of EcSSB. Purified SSB-IDL fusions bound short ssDNA oligonucleotides and exonuclease I (ExoI), an SSB interacting protein, with affinities that were strikingly similar to wild type SSB. In contrast, an SSB protein fusion with GFP directly appended to the C-terminus of SSB (SSB-C-term-GFP) failed to bind ExoI, consistent with access to the SSB-Ct being critical for SSB/protein interactions. The SSB-IDL fusions displayed defects in cooperative binding to ssDNA, reflecting the noted role for the IDL in this activity (27–30). The SSB-IDL fusions readily marked ssDNA within DNA replication reactions as demonstrated by single-molecule rolling-circle replication assays and displayed near wild type binding dynamics. Moreover, the SSB-IDL fusions supported strand-displacement synthesis by the Pol III holoenzyme, whereas SSB-C-term-GFP did not. *E. coli ssb* was successfully mutated to encode the SSB-IDL fusions as the sole SSB within *E. coli.* In contrast, transformation with a plasmid expressing SSB-C-term-GFP was not tolerated by *E. coli* carrying a second plasmid encoding wild type SSB, suggesting that direct C-terminal SSB fusions have dominant-negative effects when expressed at high levels. Strains with the SSB-IDL fusions displayed similar growth rates, protein stability, and fitness compared to those expressing wild type SSB. However, these strains were sensitized to certain DNA damaging agents and to inactivation of some DNA repair genes, indicating a modest DNA repair defect. The SSB-IDL fusions formed foci *in vivo* at frequencies that mirror those of previously studied fluorescent replication protein fusions. Collectively, the results presented highlight the utility of SSB-IDL fusion proteins for probing the functions of SSB *in vitro* and *in vivo*.

MATERIALS AND METHODS

DNA substrates and plasmids

Overexpression and complementation plasmids encoding SSB-GFP, SSB-C-term-GFP or SSB-mTur2 were created by cloning the respective open reading frames into pET21a (with T7 promoter for overexpression) or pET21a containing the *E. coli ssb* promoter (for plasmid complementation), creating pET21a-SSB-GFP, pET21a-SSB-C-term-GFP or pET21a-SSB-mTur2 (Supplementary Table S1). Plasmids were generated using Gibson cloning with oligonucleotides listed in Supplementary Table S2. For SSB-GFP and SSB-mTur2, the fluorescent proteins are positioned between residues Phe148 and Ser149. For SSB-C-term GFP, GFP immediately follows the terminal Phe of SSB. pET22b-ExoI plasmid was used for overexpression of *E. coli* ExoI with a C-terminal His-tag (11). Cy5-dT_{35} was purchased from Integrated DNA Technologies. Construction of the 2030-bp template used for the *in vitro* single-molecule rolling-circle assays has been described previously (38).

Strain construction

EAW1169 (*ssb-mTur2*) and EAW1173 (*ssb-gfp*) are *E. coli* K-12 MG1655 derivates (39). The *gfp* or *mTur2* open reading frames were inserted in the *ssb* gene between codons for Phe148 and Ser149 to encode SSB fusion proteins carrying a GFP or mTur2 domain in the IDL region. A two-step overlap PCR method (40) was used to generate PCR fragments ssb-mTur2-FRT-Kan-FRT or ssb-gfp-FRT-Kan-FRT. Briefly, plasmids pET21a-SSB-mTur2 or pET21a-SSB-GFP were used as templates to generate the first PCR *ssb-mTur2* or *ssb-gfp* fragments using primers SSBus and SSBds (Supplementary Table S2). A plasmid containing an FRT-KanR-FRT cassette was used as template to generate a second fragment homologous to 40 bp of the 3′ end of *ssb* upstream of the FRT-Kan-FRT and homologous to the 42 bp downstream of *ssb* after the FRT-Kan-FRT using primers SSBCterm and SSBafter. The two PCR products (overlapping on the 40 bp encoding the 3′ end of *ssb*) were combined and used as templates in the second step PCR with SSBus and SSBafter primers. PCR fragments were gel purified and integrated onto the chromosome using λ_{RED} recombination (41). Strains for microscopy and DNA damage sensitivity were generated by P1 transduction (42). Information on founder *Δe14* strain has been previously published (43). All constructs were confirmed by PCR or sequencing. For a full list of strains see Supplementary Table S3.

Proteins

SSBs. SSB and SSB-IDL fusions were purified as previously described (44) except that SSB-GFP, SSB-mTur2

and SSB-C-term-GFP fusions were precipitated with a final concentration of 0.195 g/mL ammonium sulfate. Protein concentrations were determined spectrophotometrically using $\varepsilon_{280} = 2.8 \times 10^4\ M^{-1}\ cm^{-1}$ for SSB (monomer) (44), $\varepsilon_{280} = 5.2 \times 10^4\ M^{-1}\ cm^{-1}$ for SSB-mTur2 (monomer), and $\varepsilon_{280} = 4.5 \times 10^4\ M^{-1}\ cm^{-1}$ for SSB-GFP or SSB-C-term GFP (monomer) (45).

ExoI. *Escherichia coli* BL21 (*DE3*) pLysS cells were transformed with pET22b-ExoI with a C-terminal His-tag (11). Cells were grown to midlog phase (OD_{600} ~0.6) at 37°C in lysogeny broth (LB) medium (46) with 50 μg/ml ampicillin and 25 μg/ml chloramphenicol. Addition of 1 mM isopropyl β-D-thiogalactopyranoside induced protein expression and cells were grown for an additional 3–4 h. Cells were resuspended in +TG buffer (50 mM Tris–HCl, pH 8.0, 0.5 M NaCl, 10% w/v glycerol, 5 mM imidazole, 0.1% v/v Triton X-100, 1 mM $MgCl_2$, and 1 protease cocktail inhibitor tablet (Pierce)) and lysed using sonication. The soluble fraction was isolated using centrifugation. Lysate was incubated with Ni-NTA agarose resin (GE) equilibrated with +TG buffer. The resin was washed with 6 column volumes of +TG buffer and 9 column volumes of –TG buffer (50 mM Tris–HCl, pH 8.0, 0.5 M NaCl, 5 mM imidazole and 1 mM $MgCl_2$). Protein was eluted after incubation with Elution buffer (50 mM Tris–HCl, pH 8.0, 0.5 M NaCl, 0.2 M imidazole, 1 mM $MgCl_2$). The concentrated ExoI eluent was further purified using a Sephacryl S-300 size exclusion column equilibrated with S300 buffer (50 mM Tris–HCl, pH 8.0, 0.5 M NaCl, 1 mM EDTA, 1 mM DTT). Pure protein was pooled and stored at −20°C in Storage buffer (50 mM Tris–HCl, pH 8.0, 0.5 M NaCl, 1 mM EDTA, 1 mM DTT, and 50% w/v glycerol). ExoI concentrations were determined spectrophotometrically using $\varepsilon_{280} = 7.3 \times 10^4\ M^{-1}\ cm^{-1}$ (11).

Replication proteins. *Escherichia coli* DNA replication proteins for *in vitro* single-molecule replication assays were produced from *E. coli* strains with genes from *E. coli* MG1655 as described previously: β_2 sliding clamp (47); $DnaB_6(DnaC)_6$ helicase–loader complex (48); DnaG primase (49); Pol III $\tau_3\delta\delta'\psi\chi$ clamp loader (50); and Pol III $\alpha\varepsilon\theta$ core (51). Pol III* [$(\alpha\varepsilon\theta)_3\tau_3\delta\delta'\psi\chi$] was assembled *in situ* using a 3:1 ratio of concentrations of $\alpha\varepsilon\theta$ and $\tau_3\delta\delta'\psi\chi$.

Microscale thermophoresis (MST)

MST binding measurements were carried out using a Monolith NT.115Pico (NanoTemper). Cy5-labeled dT_{35} was used at a final concentration of 50 pM. Measurements were carried out in 10 mM Tris–HCl, pH 8, 0.1 mM EDTA, 1 M NaCl, 0.05% Tween 20. Binding curves were fit using MO Affinity Analysis software version 1.6 (52,53) based on the binding-specific ligand induced photobleaching rate change.

Sedimentation velocity

Sedimentation velocity experiments were performed as described previously (27) with an Optima XL-A analytical ultracentrifuge and An50Ti rotor (Beckman Instruments, Fullerton, CA, USA) at 15 000 rpm (25°C).

Cy5/Cy3 labeled $(dT)_{68}$

The oligodeoxythymidylate dT_{68} doubly labeled with Cy5 and Cy3 fluorescence probes (5′-Cy5-dT_{68}-Cy3-dT-3′) was synthesized and purified as described (17) and its concentration determined spectrophotometrically in buffer T (10 mM Tris, pH 8.1, 0.1 mM Na_3EDTA) plus 0.10 M NaCl using $\varepsilon_{260} = 5.74 \times 10^5\ M^{-1}\ cm^{-1}$ (molecule) (17).

Fluorescence equilibrium titrations

The fluorescence titrations of 5′-Cy5-$(dT)_{68}$-Cy3-dT-3′) (0.1 μM) with SSB fusions (Supplementary Figure S2) were performed in buffer *T* at 25°C with NaCl concentrations of 10 mM and 0.30 M using a QM-4 spectrofluorometer (Photon Technology International/Horiba Scientific, Edison, NJ, USA) by exciting the Cy3 donor (515 nm) while monitoring the sensitized fluorescence emission from the Cy5 acceptor (665 nm) and the data were analyzed as described (29,54).

Isothermal titration calorimetry (ITC)

All measurements were performed using a VP-ITC MicroCalorimeter. SSB variants and ExoI were dialyzed at 4°C against a buffer containing 20 mM Tris–HCl, pH 8.0, 100 mM NaCl, 1 mM $MgCl_2$, 4% glycerol, 1 mM β-mercaptoethanol. SSB variants were diluted to 20 μM (monomers). ExoI (400 μM) injections (1 × 5 μl, 26 × 10 μl) were performed at 25°C. The data were fit with a single-site binding model using Origin software (Microcal).

Rolling circle-replication and FRAP

Microfluidic flow cells were prepared as described (55). Briefly, a PDMS flow chamber was placed on top of a PEG-biotin-functionalized microscope coverslip. To help prevent non-specific interactions of proteins and DNA with the surface, the chamber was blocked with buffer containing 50 mM Tris–HCl, pH 7.6, 2% Tween, 50 mM KCl. The chamber was placed on an inverted microscope (Nikon Eclipse Ti-E) with a CFI Apo TIRF 100× oil-immersion TIRF objective (NA 1.49, Nikon) and connected to a syringe pump (Adelab Scientific) for flow of buffer.

Conditions for simultaneous leading- and lagging-strand DNA replication under continuous presence of all proteins were adapted from previously described methods (34,48,51,56). Briefly, 55–300 nM $DnaB_6(DnaC)_6$ was incubated with 0.076–0.38 nM biotinylated rolling-circle template in replication buffer (25 mM Tris–HCl, pH 7.6, 10 mM magnesium acetate, 50 mM potassium glutamate, 40 μg/ml BSA, 0.1 mM EDTA, and 0.0025% Tween) with 1 mM ATP and 10 mM dithiothreitol at 37°C for 1.5 min. This mixture was diluted 10-fold and loaded into the flow cell. When optimal template density was achieved, replication was initiated by flowing in replication buffer containing 3 nM Pol III*, 30 nM β_2, 75 nM DnaG, 1.25 mM ATP, 250 μM CTP, GTP and UTP, and 50 μM dCTP, dGTP, dATP and dTTP, 10 mM dithiothreitol, and 20 nM SSB fusions (tetramers). Reactions were carried out at 31°C, maintained by an electrically heated chamber (Okolab).

Double-stranded DNA was visualized in real time by staining with 150 nM SYTOX Orange (Invitrogen) excited by a 568-nm laser (Coherent, Sapphire 568–200 CW) at 150 μW/cm^2. The SSB–GFP was excited at 700 μW/cm^2 with a 488 nm laser (Coherent, Sapphire 488–200 CW). Imaging was done with an EMCCD camera (Photometics, Evolve 512 Delta). The analysis was done with ImageJ using in-house built plugins. The rate of replication of a single molecule was obtained from its trajectory and calculated for each segment that has constant slope.

To obtain the characteristic exchange time τ from the fluorescence recovery after photobleaching (FRAP) experiments, the data were fit with a FRAP recovery function (34,51,56,57), corrected for photobleaching (Equation 1, where a is the amplitude of photobleaching, τ_b is the photobleaching time, and I_0 is the number of SSB molecules at the fork at steady state):

$$I = a * e^{-\frac{1}{\tau_b} * t} + \mathrm{I}_0 * \left(1 - e^{-\frac{1}{\tau} * t}\right) \quad (1)$$

Strand-displacement assays

Conditions for the helicase-independent Pol III strand-displacement (SD) reaction were adapted from described methods (50). Briefly, reactions contained 2 nM primed DNA template, 1 mM ATP, 0.5 mM of each dNTP, 30 nM Pol III*, 200 nM β_2 and 800 nM SSB (tetramer) (wild type or fluorescent fusion) in NaCl buffer (25 mM Tris–HCl pH 7.6, 10 mM $MgCl_2$, 10 mM dithiothreitol and 80 mM NaCl), in a final volume of 12 μl. Components (except DNA) were mixed on ice. Reactions were initiated by the addition of DNA and shifted to 37°C. Reactions were quenched at time points by addition of EDTA to ∼100 mM and SDS to ∼1% and heating to 45°C. Products were separated by 1% agarose gel electrophoresis and stained with SYBR-Gold (Invitrogen, Waltham, MA).

Plasmid complementation assay

Plasmid complementation assays were completed as previously described (44,58–60). All plasmids were validated with sequencing after passaging in liquid culture. Experiments were completed in triplicate.

Growth curves

Cultures of MG1655, EAW1169 (*ssb-mTur2*) and EAW1173 (*ssb-gfp*) were grown in flasks (using an inoculation ratio of 1:10) in LB medium at 37°C with shaking at 200 rpm. Growth was monitored by measuring OD_{600} every 30 min over 6 h. For each strain, biological triplicates were recorded. To determine the growth of each strain, the average OD_{600} of the triplicate and the corresponding standard deviation were plotted over time.

Fitness of SSB-IDL fusion strains

Fitness was determined for each fusion strain compared to the wild type using a modified growth competition assay described by Lenski *et al.* (61,62). Individual overnight cultures of *Δara* and *ara*$^+$ cells (wild type *ssb* and strains encoding SSB-IDL fusions) were grown in 3 ml LB at 37°C. The next day, a mixed culture of *Δara* and *ara*$^+$ cells was prepared with a 1:1 volume ratio. Cultures were inoculated every 24 h into 3 ml of fresh medium. The first day, 30 μl of the initial mixed culture was used as inoculum. Afterward, cultures from the previous day were used. At time 0, 24, 48 and 72 h, overnight mixed cultures were serially diluted in PBS. The dilutions were spread on tetrazolium arabinose (TA) indicator plates and incubated at 37°C for 16 h before counting. Measurements were carried out in triplicate for each combination (*ara*$^+$ and *Δara* and *vice versa*) to determine the average and the standard deviation of red and white percentage of the total population.

DNA damage sensitivity spot plates

Strains encoding SSB-GFP or SSB-mTur2 were tested for sensitivity to various DNA damaging agents. A Δ*recA* MG1655 strain was used as a DNA damage-sensitive control. Cells were grown in LB overnight at 37°C, then diluted into LB and grown to an OD_{600} of ∼1.0 and serially diluted (10^{-1} to 10^{-6}) in 0.9% (w/v) sterile NaCl, with 10 μl of dilutions spotted onto LB agar or LB agar containing a DNA damaging agent at the indicated concentration. For UV sensitivity, cells were exposed to shortwave light (254 nm) using a Spectrolinker XL-1000 UV crosslinker (Spectronics Corp) after spot plating. Images were taken after growth at 37°C overnight.

Western blot

Thirty microliters of overnight cultures of strains encoding wild type SSB (MG1655), SSB-GFP (EAW1173) or SSB-mTur2 (EAW1169) grown to saturation in LB (37°C with shaking at 200 rpm) were used as inocula to start fresh cultures that were then grown to OD_{600} = 0.2–0.3. Cells in 1 ml portions were pelleted and resuspended in 1× CB (0.5 M Tris–HCl, pH 6.8, 5% SDS, 1% glycerol, 0.5% ß-mercaptoethanol, 0.005% bromophenol blue). The volume of 1× CB buffer used for the pellet resuspension of each strain was adjusted to the OD_{600}, so that different resuspensions contained equivalent numbers of cells; 100 μl of each resuspension contained the equivalent of 1 mL of cells at OD_{600} = 1. Purified EcSSB, SSB-GFP or SSB-mTur2 were also diluted in 1× CB to 0.25 and 0.1 μM final concentrations for western blot quantification standards. Samples were heated for 10 min at 95°C, and 10 μl of samples (undiluted or diluted 5-fold) were resolved using 12% SDS-PAGE. After electrophoresis, proteins were transferred to nitrocellulose membrane for 1.5 h at 50 V. Membranes were blocked in 5% milk, 1× PBS, 0.05% Tween (5% Milk PBS-T) for 30 min at room temperature before incubation for 1.5 h in 5% Milk PBS-T with a 1:600 dilution of the primary antibody (polyclonal anti-SSB from rabbit). Membranes were washed four times for 3 min in PBS-T before incubation with the secondary antibody (anti-rabbit-HRP goat) for 45 min. Membranes were washed 4 times in 1XPBS during 3 min before visualization. Blots were visualized using SuperSignal West Pico PLUS (Thermo Scientific) and images were taken with a LAS4010 Imaging System (GE Healthcare). Biological triplicates were performed for each strain.

For SSB quantification, cells were serially diluted in PBS and 100 μl of the dilutions were spread on LB plates and incubated at 37°C for 16 h to determine cfu/mL. Protein band quantification was performed using FIJI-ImageJ. Briefly, membrane noise background was subtracted from each band signal and band intensity was first compared to the concentration of the purified proteins loaded at 0.25 μM and 0.1 μM. The average of the two comparison values was calculated to determine the protein concentrations from test strains loaded on the gel. The average of the values of the signals was used to estimate the protein concentration in each sample. This protein concentration was used to determine the number of molecules per cell. Each value reports the average with the standard deviation from biological triplicates.

SSB protein stability *in vivo*

Strains encoding wild type SSB (MG1655), SSB-GFP (EAW1173) or SSB-mTur2 (EAW1169) were grown in LB (37°C with shaking at 200 rpm). An inoculum of 110 μL of overnight culture was used to start a fresh culture of 11 mL. Cells were grown to $OD_{600} = 0.4–0.5$, then chloramphenicol was added to a final concentration of 200 μg/mL to block additional protein synthesis (63); 1 mL portions were collected after 0, 30, 60 or 120 min. Cells were pelleted then resuspended in 1XCB, with volumes adjusted as described above to ensure equivalency in the OD_{600}/resuspension volume across strains. Samples were resolved and SSB proteins detected as described above. FIJI-ImageJ was used for quantification.

Microscopy

Cells for examining focus formation, SOS induction, and nucleoid imaging were prepared as previously described (64). Cultures of SS7177, SS13186, SS13187, SS13193 and SS13195 were grown in either LB or 56/2 minimal medium supplemented with 0.4% (w/v) glucose at 37°C overnight. Three μL cultures were spotted onto 2% agarose pads made from medium with low-melting agarose and covered with a glass coverslip (65). Cells were incubated at 37°C for 2–4 h. Phase contrast and fluorescent images were taken on a Nikon E600 microscope equipped with automated filter wheels, shutters, CoolLED light source and an ORCA-ER camera. Images were taken on three different days and analyzed using OpenLabs (Improvision), Volocity (Improvision), I-Vision (BioVision), SuperSegger, Matlab R2016 and specific in-house programs written in Matlab R2019 (Mathworks).

RESULTS AND DISCUSSION

SSB-IDL fluorescent fusion proteins retain critical structural architecture

Several studies have relied on SSB fusion proteins in which a fluorescent protein is appended directly to the C-terminus of SSB (31–34,66). Given the importance of the SSB-Ct for protein interactions, these fusions can disrupt critical SSB functions. Notably, experiments that use these fusions appear to require the presence of a second wild type copy of the *ssb* gene for cell viability (31–34). This situation limits quantitative studies of SSB in bacterial cells. To attempt to alleviate this problem, SSB fluorescent fusions that maintain both the OB domain and the SSB-Ct were created and evaluated here. These EcSSB-IDL fusions contain a fluorescent protein (GFP or mTur2) inserted between Phe148 and Ser149 within the IDL (Figure 1A). We chose this insertion site due to its proximity to previously mapped regions of SSB's IDL that tolerate transposon insertions (67). A fluorescent EcSSB in which GFP is fused directly to the SSB C-terminus, similar to those used in previous studies, was also examined. Each variant was purified (Figure 1B) and tested for function *in vitro*.

Binding to Cy5-dT_{35} ssDNA was first measured to determine the DNA binding functions of the SSB variants. All measurements were recorded using microscale thermophoresis (MST) at high salt concentrations (1 M NaCl) to allow measurement of apparent dissociation constants ($K_{d,app}$). Previous studies of SSB binding to ssDNA under similar high salt conditions have reported $K_{d,app}$ values of ∼1 nM (3,68,69). Consistent with this study, EcSSB bound Cy5-dT_{35} ssDNA with $K_{d,app}$ of 1.23 ± 0.29 nM (Figure 2A). The inclusion of either GFP or mTur2 within the EcSSB IDL did not appear to impact binding: SSB-GFP and SSB-mTur2 bound ssDNA with $K_{d,app}$ values of 1.73 ± 0.26 and 1.13 ± 0.13 nM, respectively. Similarly, direct fusion of GFP to the SSB C-terminus did not appear to alter ssDNA binding ($K_{d,app}$ for SSB-C-term-GFP was 1.18 ± 0.36 nM). As expected, GFP did not bind ssDNA. Under these conditions, SSB binding to two dT_{35} molecules per tetramer can contribute to the observed DNA affinities. The SSB fusions have similar binding behavior to EcSSB and, likely, similar contributions from two dT_{35} molecules binding per tetramer.

IDL length and amino acid composition influence SSB DNA-binding and cooperativity (27,28,30). To determine if SSB-IDL fusions disrupt these functions, SSB non-nearest-neighbor cooperativity was assessed using sedimentation velocity where SSB binding to M13 bacteriophage ssDNA is detected as an increase in the average sedimentation coefficient of the DNA (27,28,30,70). A single peak in sedimentation coefficients ($s_{20,w}$) at intermediate protein-to-DNA ratios corresponds to low cooperativity. Alternatively, a bimodal distribution in the sedimentation coefficients ($s_{20,w}$) at sub-saturating SSB concentrations demonstrates highly cooperative non-nearest neighbour interactions. SSB-GFP and SSB-mTur2 lacked a clear bimodal distribution illustrating a substantial decrease in SSB non-nearest-neighbor cooperativity (Figure 2B and C). In contrast, SSB-C-term-GFP displayed bimodal behavior indicating high non-nearest neighbour cooperativity at sub-saturating concentrations ($R_{65} = 0.56$) (Figure 2D).

In addition, we used fluorescence titration studies utilizing a Cy5-$(dT)_{68}$-Cy3dT to probe SSB nearest-neighbor cooperativity (Supplementary Figure S2) (27,28,30,70). This Cy5-$(dT)_{68}$-Cy3dT substrate can accommodate either two SSB tetramers bound in the SSB_{35} mode or a single SSB tetramer in the SSB_{65} mode allowing us to assess the values of nearest-neighbor cooperativity, ω_{35}, for the SSB_{35} mode. SSB-GFP, SSB-mTur2 and SSB-C-term-GFP are all able to form both the SSB_{35} and SSB_{65} modes. Further, SSB-GFP

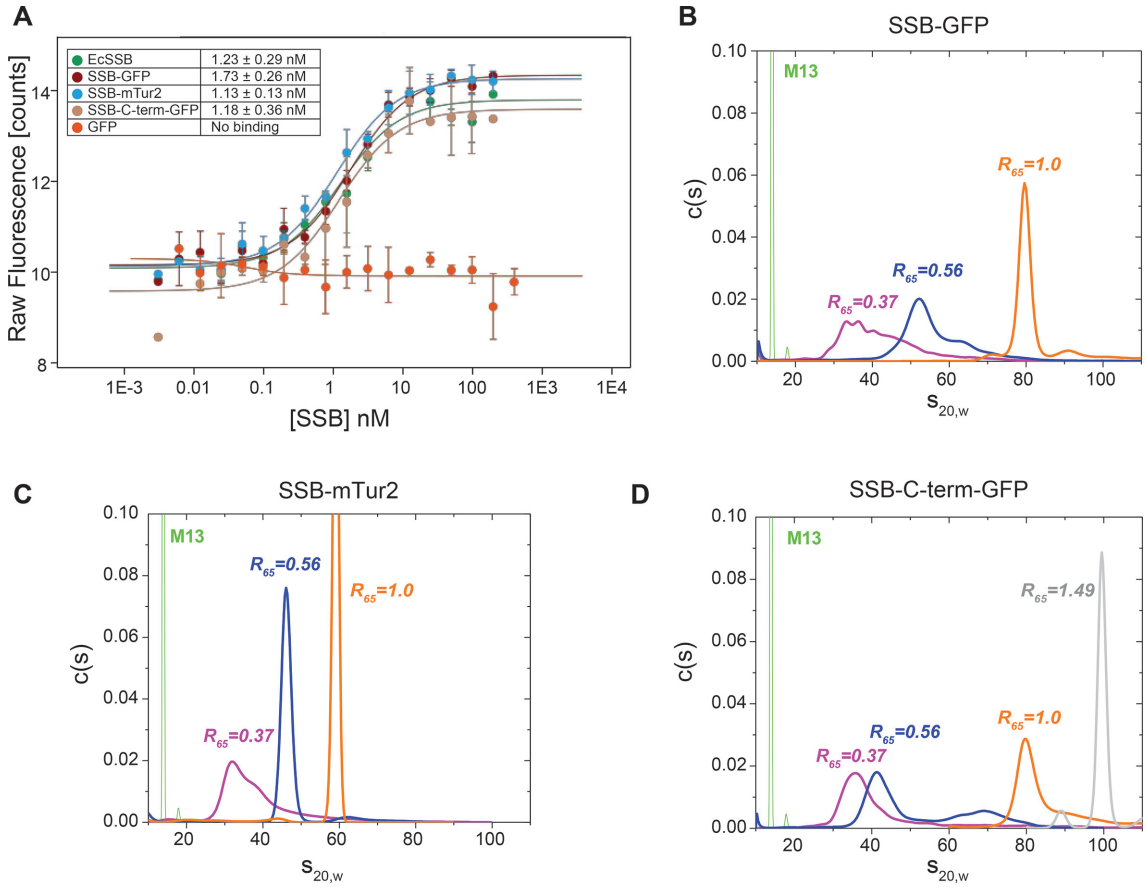

Figure 2. ssDNA binding affinities and cooperativities of EcSSB and SSB variants. (**A**) Data are presented as the mean ± standard deviation of three or more measurements. $K_{d,app}$ values are reported in the table. Binding curves were fit using MO Affinity Analysis software version 1.6 (52,53) based on the binding-specific ligand induced photobleaching rate change. Sedimentation velocity experiments of SSB-GFP (**B**), SSB-mTur2 (**C**) and SSB-C-term-GFP (**D**).

and SSB-mTur2 maintain nearest-neighbor cooperativity, albeit to a lesser extent than EcSSB or SSB-C-term-GFP. Thus, both non-nearest-neighbor and nearest-neighbor cooperativity were impacted by placement of fluorescent domains within the IDL.

To determine whether the presence of fluorescent proteins within the SSB IDL or fused to the SSB C-terminus influences SSB/protein interactions, SSB variant binding to *E. coli* ExoI was measured. SSB binds to ExoI by docking its SSB-Ct element into a pocket on ExoI (11), suggesting that direct fusions of GFP to the C-terminus of SSB could block association with ExoI. Similar SSB-Ct docking has been observed in many other SSB/protein interactions as well. The affinities of EcSSB and each of the fluorescent variants for ExoI was assessed using isothermal titration calorimetry (ITC). EcSSB and the SSB-IDL fusions bound ExoI within a very narrow range of $K_{d,app}$ values from 4.46 ± 0.51 to 5.78 ± 0.51 μM (Figure 3), indicating that the presence of either GFP or mTur2 within the SSB IDL does not disrupt SSB/ExoI complex formation. In contrast, binding of the SSB-C-term-GFP to ExoI could not be detected (Figure 3). Thus, direct fusion of GFP to the SSB C-terminus appears to disrupt SSB/ExoI interactions. This finding is consistent with previous structural and biochemical observations (9,11,17).

Functionality of SSB-IDL fusions in rolling-circle replication assays

Functionality of the SSB-IDL fusions in more complex biochemical reactions were examined next. First, EcSSB and the SSB variants were tested in a single-molecule rolling-circle replication assay (38,51,56). In this assay, the 5′-lagging-strand end of a rolling-circle substrate is tethered to the surface of a microfluidic flowcell. Replication components are introduced allowing for the assembly of replisomes and initiation of DNA synthesis. The newly synthesized leading strand is displaced and serves as the template for lagging-strand synthesis. Because of the presence of a continuous buffer flow, the generated dsDNA extension grows in the direction of flow at a rate defined by the replication velocity (Figure 4A). The dsDNA extension is visualized by staining with SYTOX orange using real-time near-total internal reflection fluorescence (TIRF) imaging (Figure 4B). Since rolling-circle replication can occur without SSB (71), these experiments are testing for potential negative consequences of including the SSB fusions. Reactions that include EcSSB had a replication rate of 626 ± 73 bp/s (N = 71) (Figure 4D) (34). Inclusion of SSB-GFP or SSB-mTur2 supported similar replication rates of 671 ± 73 s (N = 283) or 619 ± 82 s (N = 500), respectively (Figure 4C and

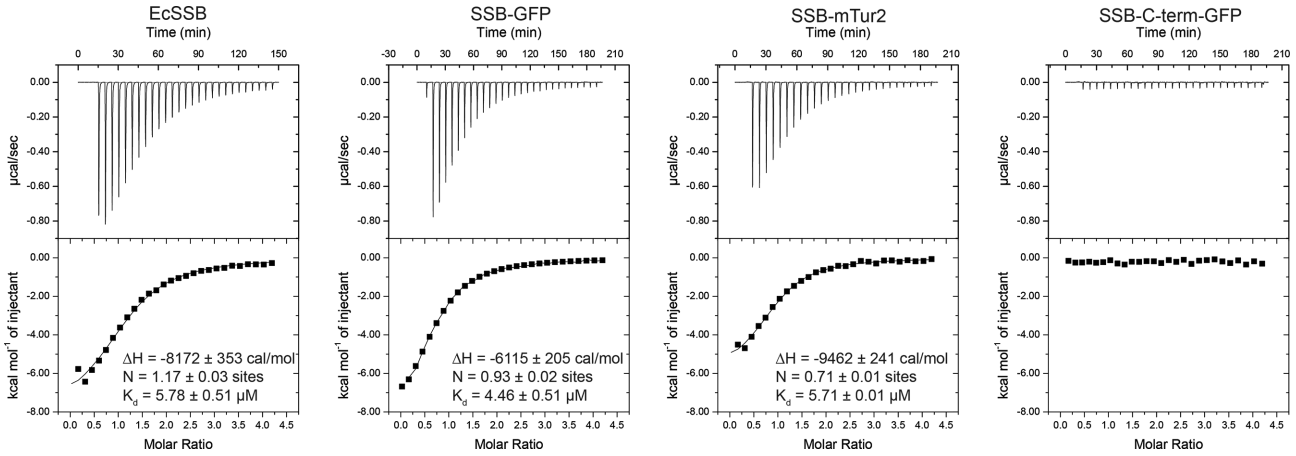

Figure 3. Interaction of EcSSB and SSB variants with ExoI determined by ITC. Heat evolved (top) and binding isotherms (bottom) from titration of the ExoI into a solution of EcSSB or SSB variants. Single-site model fit (fit line in the binding isotherm) provided the stoichiometry (*N* is the number of ExoI binding sites on each SSB monomer) and K_d for the interaction. Possible factors that may contribute to *N* values that deviate from 1.0 include the presence of minor protein contaminants that influence the accuracy of the measured protein concentration and any misfolding of purified proteins that lower interaction activity.

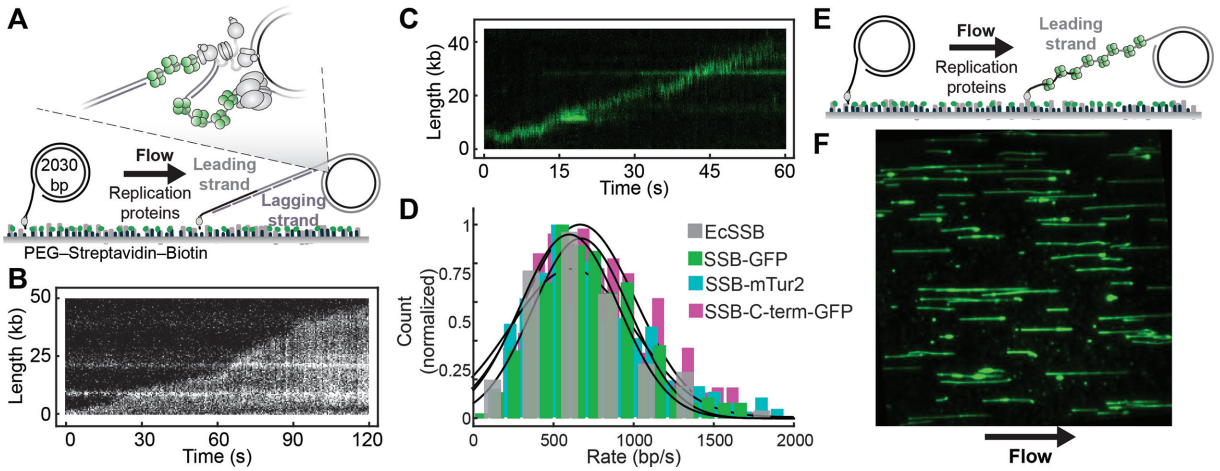

Figure 4. Single-molecule rolling-circle replication assays. (**A**) Schematic representation of the experimental design. (**B**) Kymograph of an individual DNA molecule undergoing leading- and lagging-strand replication. The gray indicates the fluorescence intensity of dsDNA stained by SYTOX orange. (**C**) Kymograph of the SSB-GFP on an individual DNA molecule. (**D**) Histograms of the rate of replication for WT SSB (626 ± 73 bp/s, $N = 71$), SSB-C-term-GFP (674 ± 80 s, $N = 372$), SSB-mTur2 (619 ± 82 bp/s, $N = 500$) and SSB-GFP (671 ± 73 bp/s, $N = 283$) fit to Gaussian distributions (black line). (**E**) Schematic representation of the experimental design for leading-strand synthesis only assays. (**F**) Representative field of view showing leading-strand synthesis products fully coated by and visualized using SSB-GFP.

D). From these data, SSB-IDL fusions do not appear to impede the reconstituted single-molecule DNA-replication reaction. Moreover, SSB-IDL fusions appeared to mark the progress of the replication fork rather than labelling the dsDNA replication product, consistent with binding selectively to exposed ssDNA at the replication fork (Figure 4C). SSB-C-term-GFP rates closely matched EcSSB and SSB-IDL fusions at 674 ± 80 s ($N = 372$) (Figure 4D).

To further assess the function of SSB-IDL fusions as a ssDNA marker, rolling-circle replication assays lacking DnaG primase, rCTP, rGTP, and rUTP were used. In this experimental setup, the RNA primers necessary for lagging-strand synthesis are not synthesized, which allows for only leading-strand synthesis and generates a ssDNA extension from the anchor (Figure 4E). Upon addition of SSB-GFP or SSB-mTur2, ssDNA extensions are readily visualized (Figure 4F, Supplementary Movie S1, and Supplementary Figure S3). Together these data demonstrate that SSB-IDL fusions can be used to monitor for the presence of ssDNA in *in vitro* replication assays.

To probe SSB-DNA binding dynamics, fluorescence recovery after photobleaching (FRAP) experiments were used to assess SSB-GFP exchange at the replication fork (Figure 5A). Due to technical limitations of the laser wavelengths used, FRAP experiments were performed only on SSB-GFP. Since mTur2 varies from GFP by only 13 residues, we predict that both SSB-IDL fusions would function similarly in these assays. Previous FRAP studies have used a single-site SSB variant (SSB-Lys43Cys) with an AlexaFluor 647 label linked at Cys43 (34). For this as-

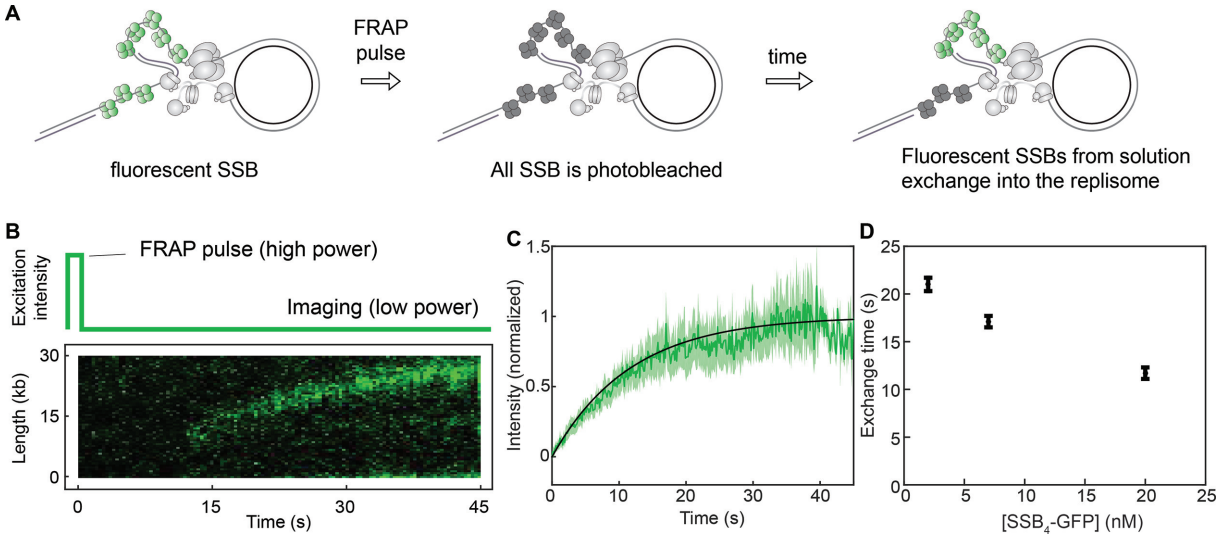

Figure 5. SSB dynamics. (**A**) Schematic representation of the FRAP experiments. SSB-GFP molecules are initially in a bright state (left). After a high intensity FRAP pulse all SSB in the field of view is photobleached (middle). If SSB is exchanged, the fluorescence should recover rapidly (right). (**B**) Imaging sequence used during the FRAP experiments (top panel). A representative kymograph of labeled SSB at the replication fork (bottom panel) in a FRAP experiment. After each FRAP pulse all SSB molecules have bleached. The fluorescence intensity recovers as unbleached SSB exchanges into the replisome. (**C**) Averaged normalized intensity for 20 nM SSB-GFP over time after a FRAP pulse. Line is a fit to (Equation 1). (**D**) Graph of exchange time at various SSB-GFP concentrations (nM). Data are presented as the mean ± standard deviation; the number of measurements is provided in the text.

say, SSB at the replication fork was periodically bleached. Bleached SSB molecules were able to exchange with bright SSB molecules in solution, and the exchange rate was monitored by the recovery of the fluorescent signal. Twenty nM SSB-Lys43Cys had an exchange rate of 5.0 ± 1.5 s (34) whereas 20 nM SSB-GFP had an exchange rate of 11.7 ± 0.6 s ($N = 59$) (Figure 5B and C). Decreasing the SSB concentration to 2 nM and 7 nM led to longer exchange rates of 21.0 ± 0.7 s ($N = 48$) and 17.1 ± 0.6 s ($N = 41$), respectively (Figure 5D). These rates closely match SSB-Lys43Cys exchange rates at 2 nM (20 ± 7 s, $N = 20$) (34). Thus, SSB-GFP dynamics at the replication fork are very similar to those of SSB AlexaFluor labeled SSB.

Since rolling-circle replication can proceed without SSB (71), a more direct test of SSB-IDL fusion function in a complex reconstituted reaction was used to better assess functionality of the fusion protein. This assay compared the abilities of SSB and SSB variants to stimulate DnaB helicase-independent strand-displacement synthesis by DNA polymerase III holoenzyme (Pol III HE). Consistent with prior observations (48,72), strand-displacement synthesis was not observed in conditions lacking EcSSB whereas in the presence of EcSSB rapid formation of long rolling-circle products were observed within 10 minutes (Supplementary Figure S4). SSB-GFP and SSB-mTur2 also support Pol III strand-displacement synthesis, albeit to a lesser extent than EcSSB (Supplementary Figure S4). Differences in the level of synthesis may be due to modest effects of the GFP and mTur2 domains on interactions between SSB-IDL fusions and the replisome. The SSB-C-term-GFP fusion does not support strand displacement synthesis under these conditions (Supplementary Figure S4), consistent with the known requirement for interaction of the SSB-Ct with the χ subunit of Pol III HE (48,72).

SSB-IDL fusions are functional *in vivo*

The utility of the SSB-IDL fusions in cellular studies was examined next. Initial experiments used a plasmid-based complementation assay to determine whether the SSB-IDL and SSB C-terminal GFP fusions were tolerated by *E. coli* and were able to complement deletion of the essential *ssb* gene (27,44,58–60). Briefly, in *E. coli* strain RDP317 the *ssb* gene has been deleted and viability is supported by the presence of a plasmid encoding EcSSB and a tetracycline-resistance gene. RDP317 was transformed with compatible, ampicillin-resistant plasmids that encode either wild type EcSSB (positive control), vector alone (negative control), or the SSB variants. Loss of the tetracycline-resistant plasmid indicates that the ampicillin-resistant plasmid encodes a functional SSB protein. Plasmids encoding either SSB-GFP or SSB-mTur2 were able to support loss of the tetracycline-resistant plasmid, indicating that they complement deletion of the chromosomal *ssb* gene. Interestingly, RPD317 cells could not be transformed with the plasmid encoding the SSB C-terminal GFP fusion, consistent with a dominant-negative phenotype in the plasmid complementation assay. This result differed from previous experiments where chromosomally-encoded SSB C-terminal GFP fusion are tolerated when a second wild type *ssb* gene is present (31–34). The difference may arise from the higher copy of the SSB C-terminal fusion in the plasmid complementation system.

To alleviate concerns about high protein levels from plasmid-expressed SSBs, mutations in the native *ssb* gene in *E. coli* MG1655 were created to encode SSB-IDL fusions *ssb-gfp* (EAW1173) or *ssb-mTur2* (EAW1169). Western blot (Figure 6C and D) and PCR analyses confirmed that these strains express only the SSB-IDL fusion without the presence of a second wild type *ssb* gene. This contrasts with pre-

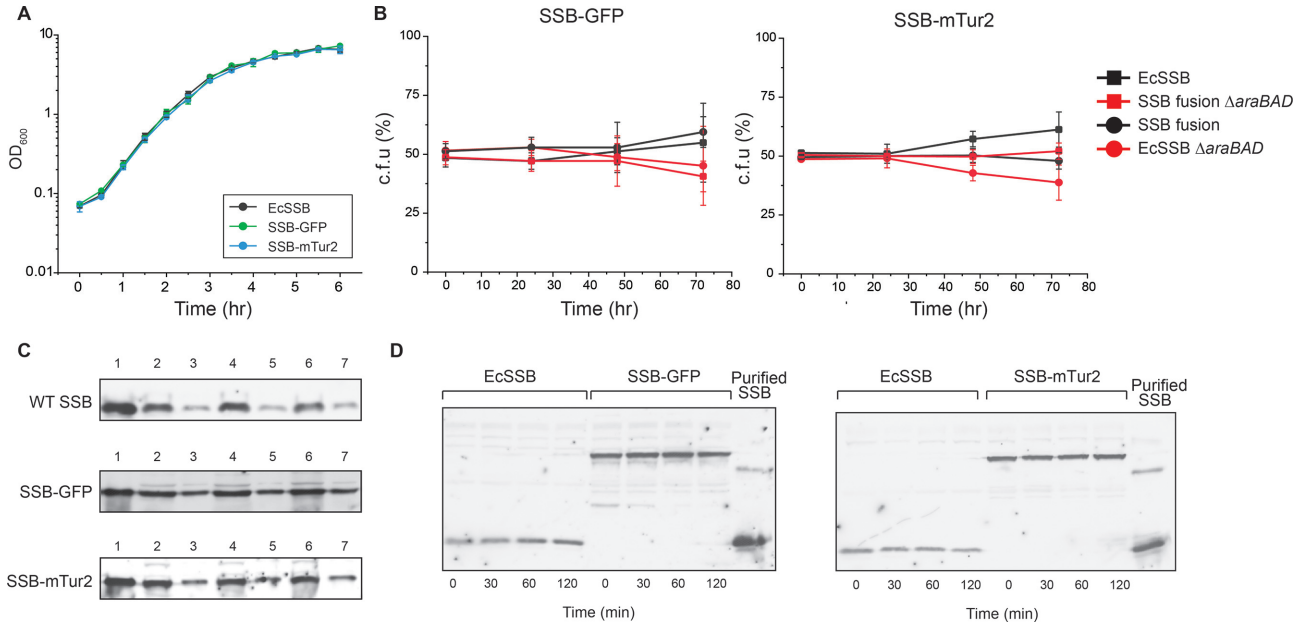

Figure 6. Characterization of *ssb-gfp* and *ssb-mTur2* strains. (**A**) Growth curves of *ssb-gfp* and *ssb-mTur2* strains compared to MG1655. (**B**) Growth competition between an EcSSB strain (MG1655) and SSB-IDL fusion strains (EAW1169 or EAW1173). Data are presented as the mean ± standard deviation of three measurements. (**C**) The protein level of EcSSB and SSB-IDL fusions produced *in vivo* was established by western blot. Image shows the signal obtained for 10 μL of 0.1 μM purified protein (column 1) compared to 10 μL of a biological triplicate of undiluted cell extract (2, 4, 6) and diluted 5 fold (3, 5, 7). (**D**) Western blot of protein stability *in vivo* over 120 min.

vious direct C-terminal SSB fusions that required the presence of a second, wild type *ssb* gene for cell viability.

To determine whether cell physiological changes accompanied chromosomal substitution of the SSB-IDL fusions in *E. coli*, growth rates and fitness were measured for EAW1173 and EAW1169. First, growth rates of both EAW1173 and EAW1169 were indistinguishable from MG1655 as measured by OD_{600} (Figure 6A), suggesting that the presence of a fluorescent domain in the SSB IDL did not affect essential cellular processes. Next, the fitness of EAW1173 and EAW1169 was probed using a two-color growth competition assay. In this assay, strains are transduced with *ara*+ or *Δara* markers, which lead to a colony color difference on tetrazolium arabinose indicator plates (62). Marked (*ara*+ *or Δara*) EAW1173 or EAW1169 cells were mixed with marked (*Δara* or *ara*+) MG1655 cells at a 1:1 ratio, then grown competitively in LB. In all instances tested, the *ara*+ or *Δara* EAW1173 and EAW1169 strains grew equally well to the *Δara* or *ara*+ MG1655 cells, indicating that that the SSB-IDL fusions did not confer a growth defect (Figure 6B).

To investigate if the presence of the SSB-IDL fusions cause DNA damage and stress *in vivo*, we utilized an *mCherry* reporter gene under the control of the *sulA* promoter to measure SOS induction (73). A control strain with wild type *ssb* did not show induction of SOS with a relative fluorescence intensity (RFI) near 1 in both rich and minimal media. Similarly, the *ssb-mTur2* fusion did not induce SOS as shown by the lack of mCherry signal with RFIs near 1 (Table 1, Supplementary Figure S5). A strain encoding *recA730-gfp* which harbors constitutive SOS was utilized as a positive control (74). This *recA* fusion was transduced into a strain containing *ssb-mTur2* and SOS induction was monitored. Constitutive SOS induction had RFIs of 10.3 ± 2.3 and 6.8 ± 1.6 for minimal and rich media conditions, respectively (Table 1). These data demonstrate that the SSB-mTur2 fusion does not induce SOS *in vivo.* Due to the similarities between *mTur2* and *gfp*, only strains with *ssb-mTur2* were examined.

Finally, SSB-GFP and SSB-mTur2 protein copy number and stability in EAW1173 and EAW1169 were assessed and compared to wild type SSB from MG1655 cells using a quantitative western-blot analysis (Figure 6C and D). MG1655 has SSB present at 2270 ± 530 molecules (monomers) per cell. Both SSB-IDL fusions had elevated SSB levels: SSB-GFP and SSB-mTur2 were present at 8200 ± 1900 and 8400 ± 1700 molecules per cell, respectively. This is consistent with the previously reported range of ∼2000 monomers/cell in minimal media with up to ∼14 400 monomers in rich media (75,76). The reason for the somewhat elevated SSB-IDL fusion protein levels is not clear. We note that genes encoding the SSB-IDL fusions maintain the promoter region of *ssb*. To measure the stability of SSB and the SSB-IDL fusions, cells were treated with chloramphenicol to block protein synthesis and protein levels over a 2 h time course were measured by western blots. No apparent degradation was observed during this time course for SSB or the SSB-IDL fusions (Figure 6D). Taken together, these data demonstrate that SSB-IDL fusions are functional and stable *in vivo*, albeit with higher levels of SSB-IDL fusion expression.

SSB-IDL fusions form foci in cells

Since SSB-GFP and SSB-mTur2 can bind ssDNA and mark replication sites *in vitro* (Figures 2 and 4), we hypothesized

Table 1. SOS induction measurements

	ssb-mTur2	*ssb-mTur2 recA730-gfp*	*ssb*
	LB		
Strain	SS13193	SS13195	SS7117
Cells counted	1978	1042	1307
RFI mCherry	1.1 ± 0.2	6.8 ± 1.6	1.2 ± 0.1
Average cell area	775.5 ± 60.8	1255.2 ± 103.3	733.6 ± 41.4
	Minimal medium		
Strain	SS13193	SS13195	SS7117
Cells counted	2293	1615	1683
RFI mCherry	1.0 ± 0.3	10.3 ± 2.3	1.1 ± 0.3
Average cell area	539.0 ± 119.5	830.0 ± 134.9	437.3 ± 68.9

For strain information see Supplementary Table S3. mCherry relative fluorescence intensity (RFI) was a measure for SOS induction.

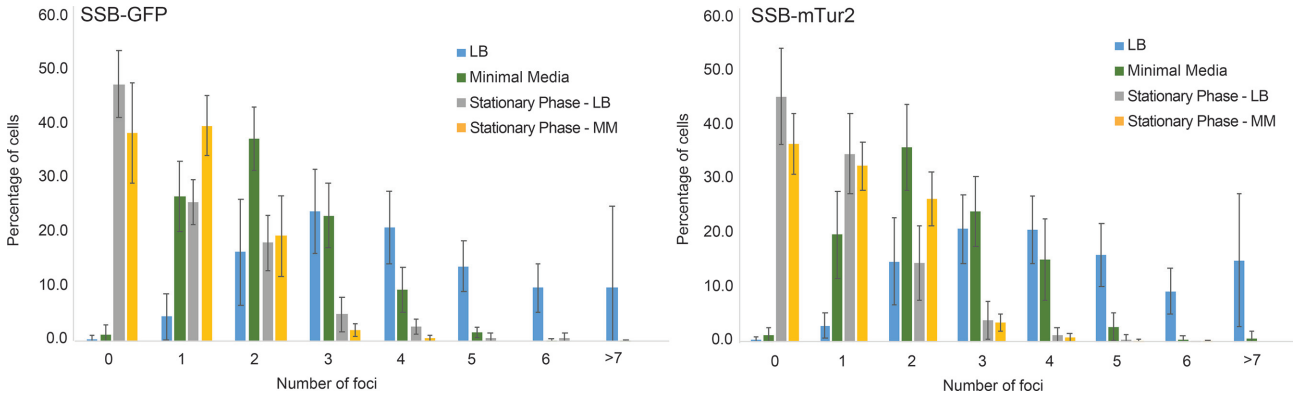

Figure 7. Fluorescent focus formation in *ssb-gfp* and *ssb-mtur2* cells. Values are the percent of cells with a given number of foci. Data are presented as the mean ± standard deviation; the number of cells analyzed is provided in the text.

that they would form foci at sites of DNA replication or other exposed ssDNA in *E. coli.* To test this, strains expressing SSB-GFP and SSB-mTur2 were visualized using fluorescence microscopy. An additional fluorescent fusion protein (HupA-mCherry) was used in conjunction with the SSB-IDL fusions to identify nucleoids (77,78). SSB-GFP and SSB-mTur2 foci were readily observed and were nearly always localized to nucleoid regions of cells (Supplementary Figure S6).

Next, the number of SSB foci in cells was quantified in different growth media. We predicted that cells would have higher numbers of SSB-IDL fusion foci in rich media, where replication is more frequent, than in minimal medium. Consistent with this prediction, SSB-GFP- and SSB-mTur2-expressing cells had an average of 4.1 ± 1.0 (N = 1510) and 4.4 ± 0.9 (N = 1441) foci per cell, respectively, in rich medium and 2.2 ± 0.2 (N = 2746) and 2.5 ± 0.3 (N = 1952) foci per cell in minimal medium supplemented with glucose (Figures 7 and 8). These frequencies were very similar to those reported for fluorescently-tagged replication fusion proteins (57,79,80), suggesting that the SSB foci likely mark sites of DNA replication. Additionally, as expected for a non-replicative state, SSB-GFP- and SSB-mTur2-expressing cells in stationary phase had greatly reduced numbers of foci per cell (Figure 7). Stationary phase SSB-GFP-expressing cells had 0.9 ± 0.1 (N = 869; LB) or 0.9 ± 0.1 (N = 1503; minimal medium) foci per cell and SSB-mTur2-expressing cells had 0.8 ± 0.3 (N = 1188; LB) or 1.0 ± 0.1 (N = 1908; minimal medium) foci per cell (Figure 7). Together, these data demonstrate that SSB-IDL fusions form foci in cells that closely matching the frequency of replication fork focus formation.

Function of SSB-IDL fusions in DNA repair

To determine whether inclusion of GFP or mTur2 in the IDL of SSB alters cellular DNA repair activities, strains with chromosomally-incorporated *ssb-gfp* and *ssb-mtur2* genes were tested for sensitivity to DNA damaging agents. The strains were compared to a control *ΔrecA* strain that was previously demonstrated to be highly sensitive to DNA damage (81,82). SSB-GFP and SSB-mTur2 strains displayed normal sensitivity to treatment by ciprofloxacin, mitomycin C, and bleomycin (Figure 9). In contrast, the strains were sensitized to treatment with nitrofurantoin (at 4 or 6 μM, but not 2 μM) and UV (at 20 or 40 J/m^2, but not 10 J/m^2), whereas the control *ΔrecA* strain had greatly limited or no growth under these conditions (Figure 9). Finally, the strains were mildly sensitive to high doses of trimethoprim. Interestingly, when SSB-IDL fusions are expressed from a plasmid yielding higher copy numbers, increased DNA damage sensitivity to all agents tested was observed (Supplementary Figure S7), suggesting that the SSB-IDL protein levels may have an impact on DNA damage sensitivity. These data suggest that the SSB-IDL fusions generally support DNA repair pathways with some exceptions where the fusions may somewhat limit repair. However, the defects are substantially less than those observed in strains lacking RecA function.

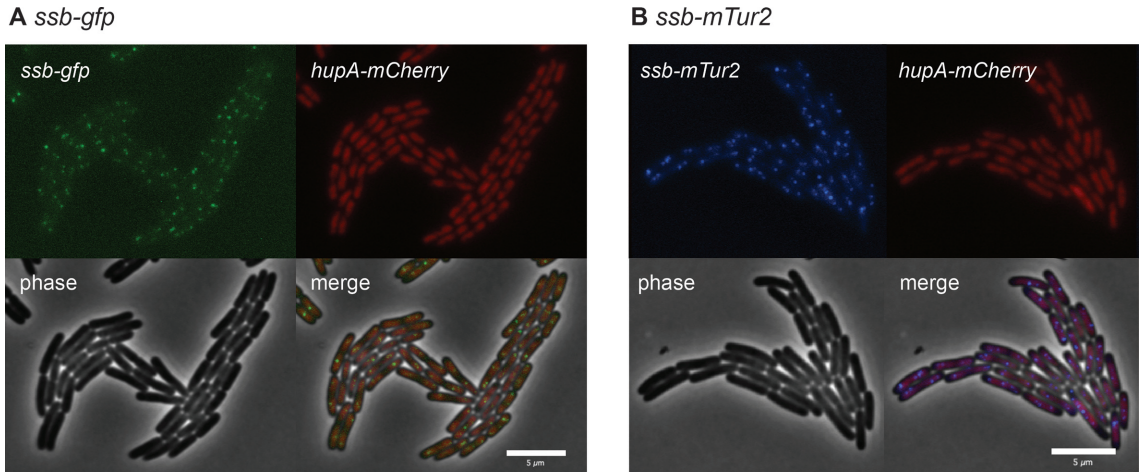

Figure 8. Representative images of SSB fusion strains in minimal medium supplemented with glucose. (**A**) *ssb-gfp* fusion. (**B**) *ssb-mtur2* fusion. Nucleoids are visualized using a *hupA-mCherry* fusion. Scale bar is 5 μm.

To further probe the impact of the SSB-IDL fusions on cellular DNA maintenance processes, strains containing combinations of SSB-IDL fusions and DNA repair gene deletions were generated and tested for sensitivity to damage induced by nitrofurantoin and UV light. SSB-IDL fusions had the largest synergistic effects with deletions of *recJ*, *sbcB* (encodes ExoI), and *recB* with both UV and nitrofurantoin treatment (Supplementary Figure S8). RecJ, ExoI and RecB(CD) process DNA repair substrates, a process that may be impaired in the presence of our SSB-IDL fusions (83). The effect with the *sbcB* strains was intriguing since both SSB-IDL fusions bind ExoI with near wild type affinity *in vitro* (Figure 3). This discrepancy may arise from requirements for the SSB/ExoI complex in cells that are not simply a function of interaction in the direct interaction assay used in our study. More minor effects were also observed with SSB-IDL fusions combined with deletions of the *recFOR* genes and *uvrA*. Further, a minor rescue of the SSB-IDL fusion sensitivity to nitrofurantoin was observed with a deletion of *mutS*.

There are multiple possibilities that could explain the DNA repair phenotypes of strains containing the SSB-IDL fusions. First, SSB-IDL fusions were defective in non-nearest-neighbor and nearest-neighbor cooperativity. SSB cooperativity may be important for SSB function in DNA repair pathways, and these defects may have an effect on SSB function *in vivo* as suggested previously (29,58). Second, the differences in cellular concentration of SSB-IDL fusions (∼8000 monomers) compared to wild type SSB (∼2000 monomers) may have an impact on SSB function by titrating SSB interacting proteins away from their sites of action. Indeed, overexpression of SSB has been shown to induce DNA damage in *E. coli* (84). Third, the presence of the fluorescent domains within the IDL could prevent proper IDL function. Several proteins containing intrinsically disordered regions have been shown to form membrane-less organelles via phase separation. Previous work has suggested that SSB may also form phase-separated species (85,86). The IDL region of SSB could potentially mediate phase separation that is important for some DNA repair processes and insertion of fluorescent domains within the IDL could disrupt this phenomenon. In a related potential effect, SSB's IDL have been shown to function in DNA-binding cooperativity (27,30,87). Additionally, SSB IDLs have been proposed to function in protein-protein interactions (87) although a study showing that *E. coli* SSB variants lacking the IDL retain binding to several SSB binding partners (17) does not support this proposal. Introduction of fluorescent domains within the IDL could limit cooperative DNA binding or block certain SSB-protein interactions, which may be important for specific DNA repair circumstances. Finally, the size of the fluorescent domain may physically block specific repair pathways or impede interactions with a subset of SSB interacting proteins. It will be interesting to probe the cellular mechanisms underlying the specific sensitivities observed here and the potential involvement of phase separation in SSB function.

SUMMARY

Novel SSB fluorescent fusions that are functional both *in vitro* and in *E. coli* cells are now available for genome maintenance studies. These fusion proteins support activities in reconstituted replication reactions *in vitro*. Furthermore, the proteins allow cell viability without the need for an additional wild type *ssb* gene. Strains expressing SSB-IDL fusions do have modest sensitivity to some DNA damaging agents. Nonetheless, due to their functionality in *E. coli* these probes will be of great use in probing cellular functions of SSB. Moreover, the SSB-IDL fusions will allow direct comparison of SSB activity in cellular and biochemical studies since, unlike direct C-terminal SSB fusions or chemically labelled SSBs, these fusions can be used both *in vivo* and *in vitro*. Recently, fluorescent fusions of RPA (the human homolog of SSB) have been used in single-molecule DNA curtain experiments to identify mechanisms of eukaryotic recombination (88). We propose that the SSB-IDL fusions will enable analogous probing of bacterial recombination and repair pathways.

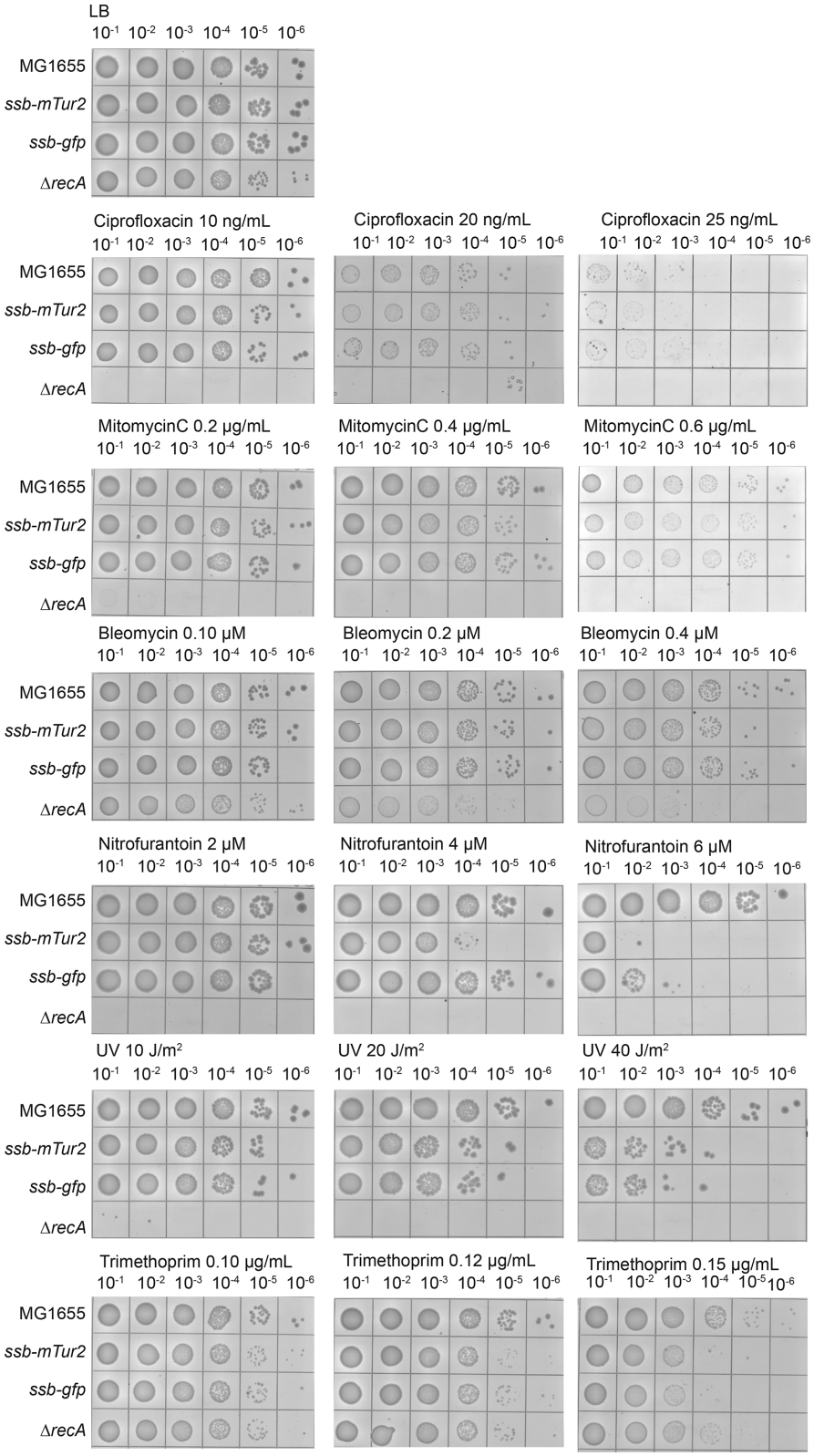

Figure 9. Sensitivity to DNA damaging agents. The *ΔrecA* strain is used as a DNA damage hypersensitive control.

DATA AVAILABILITY

Home-built ImageJ plugins have been deposited on the Github repository for Single-molecule/Image analysis tools (https://github.com/SingleMolecule). Overexpression plasmids pET21a-SSB-GFP, pET21a-SSB-C-term-GFP, and pET21a-SSB-mTur2 have been deposited with AddGene with ID numbers of 136471, 136472, and 136473, respectively.

SUPPLEMENTARY DATA

Supplementary Data are available at NAR Online.

ACKNOWLEDGEMENTS

We thank the researchers in the Keck, Cox, van Oijen, Lohman, Dixon and Sandler laboratories for critical evaluations of the manuscript.

FUNDING

National Institutes of Health [R01 GM098885 to J.L.K., S.J.S., RM1 GM130450 to M.M.C, J.L.K., A.M.v.O., R01 GM030498 to T.M.L.]; Australian Research Council [FL140100027 to A.M.v.O., DP180100858 to A.M.v.O. and N.E.D.]; the Monolith NT.115Pico was purchased by the Medicinal Chemistry Center at the University of Wisconsin – Madison, School of Pharmacy with a UW2020 instrumentation grant made possible by the Vice Chancellor for Research and Graduate Education and funded by WARF; ITC data were obtained at the University of Wisconsin – Madison Biophysics Instrumentation Facility, which was established with support from the University of Wisconsin – Madison [BIR-9512577 (NSF) and S10 RR13790 (NIH)]. The open access publication charge for this paper has been waived by Oxford University Press – *NAR* Editorial Board members are entitled to one free paper per year in recognition of their work on behalf of the journal.
Conflict of interest statement. None declared.

REFERENCES

1. Shereda,R.D., Kozlov,A.G., Lohman,T.M., Cox,M.M. and Keck,J.L. (2008) SSB as an organizer/mobilizer of genome maintenance complexes. *Crit. Rev. Biochem. Mol. Biol.*, **43**, 289–318.
2. Molineux,I.J. and Gefter,M.L. (1975) Properties of the Escherichia coli DNA-binding (unwinding) protein interaction with nucleolytic enzymes and DNA. *J. Mol. Biol.*, **98**, 811–825.
3. Molineux,I.J., Pauli,A. and Gefter,M.L. (1975) Physical studies of the interaction between the Escherichia coli DNA binding protein and nucleic acids. *Nucleic Acids Res.*, **2**, 1821–1838.
4. Meyer,R.R. and Laine,P.S. (1990) The single-stranded DNA-binding protein of Escherichia coli. *Microbiol. Rev.*, **54**, 342–380.
5. Chase,J.W. and Williams,K.R. (1986) Single-stranded DNA binding proteins required for DNA replication. *Ann. Rev. Biochem.*, **55**, 103–136.
6. Shereda,R.D., Reiter,N.J., Butcher,S.E. and Keck,J.L. (2009) Identification of the SSB binding site on E. coli RecQ reveals a conserved surface for binding SSB's C terminus. *J. Mol. Biol.*, **386**, 612–625.
7. Cadman,C.J. and McGlynn,P. (2004) PriA helicase and SSB interact physically and functionally. *Nucleic Acids Res.*, **32**, 6378–6387.
8. Chen,S.H., Byrne-Nash,R.T. and Cox,M.M. (2016) Escherichia coli RadD protein functionally interacts with the single-stranded DNA-binding protein. *J. Biol. Chem.*, **291**, 20779–20786.
9. Kozlov,A.G., Jezewska,M.J., Bujalowski,W. and Lohman,T.M. (2010) Binding specificity of Escherichia coli single-stranded DNA binding protein for the χ subunit of DNA pol III holoenzyme and PriA helicase. *Biochemistry*, **49**, 3555–3566.
10. Lecointe,F., Serena,C., Velten,M., Costes,A., McGovern,S., Meile,J.C., Errington,J., Ehrlich,S.D., Noirot,P. and Polard,P. (2007) Anticipating chromosomal replication fork arrest: SSB targets repair DNA helicases to active forks. *EMBO J.*, **26**, 4239–4251.
11. Lu,D. and Keck,J.L. (2008) Structural basis of Escherichia coli single-stranded DNA-binding protein stimulation of exonuclease I. *Proc. Natl Acad. Sci. U.S.A.*, **105**, 9169–9174.
12. Page,A.N., George,N.P., Marceau,A.H., Cox,M.M. and Keck,J.L. (2011) Structure and biochemical activities of Escherichia coli MgsA. *J. Biol. Chem.*, **286**, 12075–12085.
13. Petzold,C., Marceau,A.H., Miller,K.H., Marqusee,S. and Keck,J.L. (2015) Interaction with single-stranded DNA-binding protein stimulates Escherichia coli ribonuclease HI enzymatic activity. *J. Biol. Chem.*, **290**, 14626–14636.
14. Shereda,R.D., Bernstein,D.A. and Keck,J.L. (2007) A central role for SSB in Escherichia coli RecQ DNA helicase function. *J. Biol. Chem.*, **282**, 19247–19258.
15. Wessel,S.R., Marceau,A.H., Massoni,S.C., Zhou,R., Ha,T., Sandler,S.J. and Keck,J.L. (2013) PriC-mediated DNA replication restart requires PriC complex formation with the single-stranded DNA-binding protein. *J. Biol. Chem.*, **288**, 17569–17578.
16. Curth,U., Genschel,J., Urbanke,C. and Greipel,J. (1996) In vitro and in vivo function of the C-terminus of Escherichia coli single-stranded DNA binding protein. *Nucleic Acids Res.*, **24**, 2706–2711.
17. Shinn,M.K., Kozlov,A.G., Nguyen,B., Bujalowski,W.M. and Lohman,T.M. (2019) Are the intrinsically disordered linkers involved in SSB binding to accessory proteins? *Nucleic Acids Res.*, **47**, 8581–8594.
18. Chan,K.-W., Lee,Y.-J., Wang,C.-H., Huang,H. and Sun,Y.-J. (2009) Single-stranded DNA-binding protein complex from Helicobacter pylori suggests an ssDNA-binding surface. *J. Mol. Biol.*, **388**, 508–519.
19. Huang,Y.-H., Guan,H.-H., Chen,C.-J. and Huang,C.-Y. (2017) Staphylococcus aureus single-stranded DNA-binding protein SsbA can bind but cannot stimulate PriA helicase. *PLoS One*, **12**, e0182060.
20. Jędrzejczak,R., Dauter,M., Dauter,Z., Olszewski,M., Długołęcka,A. and Kur,J. (2006) Structure of the single-stranded DNA-binding protein SSB from Thermus aquaticus. *Acta Cryst. D*, **62**, 1407–1412.
21. Kaushal,P.S., Singh,P., Sharma,A., Muniyappa,K. and Vijayan,M. (2010) X-ray and molecular-dynamics studies on Mycobacterium leprae single-stranded DNA-binding protein and comparison with other eubacterial SSB structures. *Acta Cryst. D*, **66**, 1048–1058.
22. Matsumoto,T., Morimoto,Y., Shibata,N., Kinebuchi,T., Shimamoto,N., Tsukihara,T. and Yasuoka,N. (2000) Roles of functional loops and the CD-terminal segment of a single-stranded DNA binding protein elucidated by X-ray structure analysis. *J. Biochem.*, **127**, 329–335.
23. Raghunathan,S., Kozlov,A.G., Lohman,T.M. and Waksman,G. (2000) Structure of the DNA binding domain of E. coli SSB bound to ssDNA. *Nat. Struct. Biol.*, **7**, 648–652.
24. Raghunathan,S., Ricard,C.S., Lohman,T.M. and Waksman,G. (1997) Crystal structure of the homo-tetrameric DNA binding domain of Escherichia coli single-stranded DNA-binding protein determined by multiwavelength x-ray diffraction on the selenomethionyl protein at 2.9-Å resolution. *Proc. Natl Acad. Sci. U.S.A.*, **94**, 6652–6657.
25. Saikrishnan,K., Jeyakanthan,J., Venkatesh,J., Acharya,N., Sekar,K., Varshney,U. and Vijayan,M. (2003) Structure of Mycobacterium tuberculosis single-stranded DNA-binding protein. Variability in quaternary structure and its implications. *J. Mol. Biol.*, **331**, 385–393.
26. Savvides,S.N., Raghunathan,S., Fütterer,K., Kozlov,A.G., Lohman,T.M. and Waksman,G. (2004) The C-terminal domain of full-length E. coli SSB is disordered even when bound to DNA. *Protein Sci.*, **13**, 1942–1947.
27. Kozlov,A.G., Weiland,E., Mittal,A., Waldman,V., Antony,E., Fazio,N., Pappu,R.V. and Lohman,T.M. (2015) Intrinsically disordered C-terminal tails of E. coli single-stranded DNA binding protein regulate cooperative binding to single-stranded DNA. *J. Mol. Biol.*, **427**, 763–774.

28. Antony,E. and Lohman,T.M. (2019) Dynamics of E. coli single stranded DNA binding (SSB) protein-DNA complexes. *Semin. Cell Dev. Biol.*, **86**, 102–111.
29. Kozlov,A.G., Shinn,M.K. and Lohman,T.M. (2019) Regulation of Nearest-Neighbor cooperative binding of E. coli SSB protein to DNA. *Biophys. J.*, **117**, 2120–2140.
30. Kozlov,A.G., Shinn,M.K., Weiland,E.A. and Lohman,T.M. (2017) Glutamate promotes SSB protein-protein Interactions via intrinsically disordered regions. *J. Mol. Biol.*, **429**, 2790–2801.
31. Reyes-Lamothe,R. (2012) In: Keck,JL (ed.) *Single-Stranded DNA Binding Proteins: Methods and Protocols*. Humana Press, Totowa, pp. 245–253.
32. Reyes-Lamothe,R., Possoz,C., Danilova,O. and Sherratt,D.J. (2008) Independent positioning and action of Escherichia coli replisomes in live cells. *Cell*, **133**, 90–102.
33. Reyes-Lamothe,R., Sherratt,D.J. and Leake,M.C. (2010) Stoichiometry and architecture of active DNA replication machinery in Escherichia coli. *Science*, **328**, 498–501.
34. Spenkelink,L.M., Lewis,J.S., Jergic,S., Xu,Z.-Q., Robinson,A., Dixon,N.E. and van Oijen,A.M. (2019) Recycling of single-stranded DNA-binding protein by the bacterial replisome. *Nucleic Acids Res.*, **47**, 4111–4123.
35. Kim,Y., Ho,S.O., Gassman,N.R., Korlann,Y., Landorf,E.V., Collart,F.R. and Weiss,S. (2008) Efficient site-specific labeling of proteins via cysteines. *Bioconj. Chem.*, **19**, 786–791.
36. Hedgethorne,K. and Webb,M.R. (2012) In: Keck,JL (ed.) *Single-Stranded DNA Binding Proteins: Methods and Protocols*. Humana Press, Totowa, pp. 219–233.
37. Suksombat,S., Khafizov,R., Kozlov,A.G., Lohman,T.M. and Chemla,Y.R. (2015) Structural dynamics of E. coli single-stranded DNA binding protein reveal DNA wrapping and unwrapping pathways. *Elife*, **4**, e08193.
38. Monachino,E., Ghodke,H., Spinks,R.R., Hoatson,B.S., Jergic,S., Xu,Z.-Q., Dixon,N.E. and van Oijen,A.M. (2018) Design of DNA rolling-circle templates with controlled fork topology to study mechanisms of DNA replication. *Anal. Biochem.*, **557**, 42–45.
39. Blattner,F.R., Plunkett,G., Bloch,C.A., Perna,N.T., Burland,V., Riley,M., Collado-Vides,J., Glasner,J.D., Rode,C.K., Mayhew,G.F. *et al.* (1997) The complete genome sequence of *Escherichia coli* K-12. *Science*, **277**, 1453–1462.
40. Horton,R.M. (1995) PCR-mediated recombination and mutagenesis. *Mol. Biotech.*, **3**, 93–99.
41. Datsenko,K.A. and Wanner,B.L. (2000) One-step inactivation of chromosomal genes in *Escherichia coli* K-12 using PCR products. *Proc. Natl Acad. Sci. U.S.A.*, **97**, 6640–6645.
42. Thomason,L.C., Costantino,N. and Court,D.L. (2007) E. coli genome manipulation by P1 transduction. *Curr. Protocol. Mol. Biol.*, **79**, 1.17.11–11.17.18.
43. Bruckbauer,S.T., Trimarco,J.D., Martin,J., Bushnell,B., Senn,K.A., Schackwitz,W., Lipzen,A., Blow,M., Wood,E.A., Culberson,W.S. *et al.* (2019) Experimental evolution of extreme resistance to ionizing radiation in Escherichia coli after 50 cycles of selection. *J. Bact.*, **201**, e00784-00718.
44. Dubiel,K., Myers,A.R., Kozlov,A.G., Yang,O., Zhang,J., Ha,T., Lohman,T.M. and Keck,J.L. (2019) Structural mechanisms of cooperative DNA binding by bacterial Single-Stranded DNA-Binding proteins. *J. Mol. Biol.*, **431**, 178–195.
45. Gill,S.C. and von Hippel,P.H. (1989) Calculation of protein extinction coefficients from amino acid sequence data. *Anal. Biochem.*, **182**, 319–326.
46. Sambrook,J. and Russell,D. (2001) *Molecular cloning: a laboratory manual*. Cold Spring Harbor Laboratory Press, Vol. **1**, p. 2100.
47. Oakley,A.J., Prosselkov,P., Wijffels,G., Beck,J.L., Wilce,M.C. and Dixon,N.E. (2003) Flexibility revealed by the 1.85 Å crystal structure of the β sliding-clamp subunit of Escherichia coli DNA polymerase III. *Acta Cryst. D*, **59**, 1192–1199.
48. Jergic,S., Horan,N.P., Elshenawy,M.M., Mason,C.E., Urathamakul,T., Ozawa,K., Robinson,A., Goudsmits,J.M., Wang,Y. and Pan,X. (2013) A direct proofreader–clamp interaction stabilizes the Pol III replicase in the polymerization mode. *EMBO J.*, **32**, 1322–1333.
49. Stamford,N.P.J., Stamford,J., Lilley,P.E. and Dixon,N.E. (1992) Enriched sources of Escherichia coli replication proteins: the dnaG primase is a zinc metalloprotein. *Biochim. Biophys. Acta*, **1132**, 17–25.
50. Tanner,N.A., Hamdan,S.M., Jergic,S., Loscha,K.V., Schaeffer,P.M., Dixon,N.E. and Van Oijen,A.M. (2008) Single-molecule studies of fork dynamics in Escherichia coli DNA replication. *Nat. Stuct. Mol. Biol.*, **15**, 170.
51. Lewis,J.S., Spenkelink,L.M., Jergic,S., Wood,E.A., Monachino,E., Horan,N.P., Duderstadt,K.E., Cox,M.M., Robinson,A. and Dixon,N.E. (2017) Single-molecule visualization of fast polymerase turnover in the bacterial replisome. *Elife*, **6**, e23932.
52. Jerabek-Willemsen,M., André,T., Wanner,R., Roth,H.M., Duhr,S., Baaske,P. and Breitsprecher,D. (2014) MicroScale thermophoresis: interaction analysis and beyond. *J. Mol. Struct.*, **1077**, 101–113.
53. Zillner,K., Jerabek-Willemsen,M., Duhr,S., Braun,D., Längst,G. and Baaske,P. (2012) *Functional Genomics*. Springer, pp. 241–252.
54. Kozlov,A.G., Galletto,R. and Lohman,T.M. (2012) In Keck,JL (ed.) *Single-Stranded DNA Binding Proteins: Methods and Protocols*. Humana Press, Totowa, pp. 55–83.
55. Geertsema,H.J., Duderstadt,K.E. and van Oijen,A.M. (2015) *DNA Replication*. Springer, pp. 219–238.
56. Tanner,N.A., Loparo,J.J., Hamdan,S.M., Jergic,S., Dixon,N.E. and van Oijen,A.M. (2009) Real-time single-molecule observation of rolling-circle DNA replication. *Nucleic Acids Res.*, **37**, e27.
57. Beattie,T.R., Kapadia,N., Nicolas,E., Uphoff,S., Wollman,A.J., Leake,M.C. and Reyes-Lamothe,R. (2017) Frequent exchange of the DNA polymerase during bacterial chromosome replication. *Elife*, **6**, e21763.
58. Antony,E., Weiland,E., Yuan,Q., Manhart,C.M., Nguyen,B., Kozlov,A.G., McHenry,C.S. and Lohman,T.M. (2013) Multiple C-terminal tails within a single E. coli SSB homotetramer coordinate DNA replication and repair. *J. Mol. Biol.*, **425**, 4802–4819.
59. Carlini,L.E., Porter,R.D., Curth,U. and Urbanke,C. (1993) Viability and preliminary in vivo characterization of site directed mutants of Escherichia coli single-stranded DNA-binding protein. *Mol Micro*, **10**, 1067–1075.
60. Porter,R.D. and Black,S. (1991) The single-stranded-DNA-binding protein encoded by the Escherichia coli F factor can complement a deletion of the chromosomal ssb gene. *J Bact*, **173**, 2720–2723.
61. Kim,T., Chitteni-Pattu,S., Cox,B.L., Wood,E.A., Sandler,S.J. and Cox,M.M. (2015) Directed evolution of RecA variants with enhanced capacity for conjugational recombination. *PLos Genet.*, **11**, e1005278.
62. Lenski,R.E., Rose,M.R., Simpson,S.C. and Tadler,S.C. (1991) Long-term experimental evolution in Escherichia coli. I. Adaptation and divergence during 2,000 generations. *Amer Naturalist*, **138**, 1315–1341.
63. Battesti,A., Hoskins,J.R., Tong,S., Milanesio,P., Mann,J.M., Kravats,A., Tsegaye,Y.M., Bougdour,A., Wickner,S. and Gottesman,S. (2013) Anti-adaptors provide multiple modes for regulation of the RssB adaptor protein. *Genes Dev.*, **27**, 2722–2735.
64. Warr,A.R., Klimova,A.N., Nwaobasi,A.N. and Sandler,S.J. (2019) Protease-deficient SOS constitutive cells have RecN-dependent cell division phenotypes. *Mol Micro*, **111**, 405–422.
65. Levin,P.A. (2002) Light microscopy techniques for bacterial cell biology. *Methods Microbiol.*, **31**, 115–132.
66. Zhao,T., Liu,Y., Wang,Z., He,R., Xiang Zhang,J., Xu,F., Lei,M., Deci,M.B., Nguyen,J. and Bianco,P.R. (2019) Super-resolution imaging reveals changes in Escherichia coli SSB localization in response to DNA damage. *Genes Cells*, **24**, 814–826.
67. Goodall,E.C., Robinson,A., Johnston,I.G., Jabbari,S., Turner,K.A., Cunningham,A.F., Lund,P.A., Cole,J.A. and Henderson,I.R. (2018) The essential genome of Escherichia coli K-12. *MBio*, **9**, e02096-02017.
68. Lohman,T.M. and Overman,L.B. (1985) Two binding modes in Escherichia coli single strand binding protein-single stranded DNA complexes. Modulation by NaCl concentration. *J. Biol. Chem.*, **260**, 3594–3603.
69. Krauss,G., Sindermann,H., Schomburg,U. and Maass,G. (1981) Escherichia coli single-strand deoxyribonucleic acid binding protein: stability, specificity, and kinetics of complexes with oligonucleotides and deoxyribonucleic acid. *Biochem*, **20**, 5346–5352.
70. Bujalowski,W. and Lohman,T.M. (1989) Negative co-operativity in Escherichia coli single strand binding protein-oligonucleotide interactions: II. Salt, temperature and oligonucleotide length effects. *J. Mol. Biol.*, **207**, 269–288.

71. Mok,M. and Marians,K. (1987) The Escherichia coli preprimosome and DNA B helicase can form replication forks that move at the same rate. *J. Biol. Chem.*, **262**, 16644–16654.
72. Yuan,Q. and McHenry,C.S. (2009) Strand displacement by DNA polymerase III occurs through a τ-ψ-χ link to single-stranded DNA-binding protein coating the lagging strand template. *J. Biol. Chem.*, **284**, 31672–31679.
73. Simmons,L.A., Foti,J.J., Cohen,S.E. and Walker,G.C. (2008) The SOS regulatory network. *EcoSal Plus*, **2008**, doi:10.1128/ecosalplus.5.4.3.
74. Lavery,P.E. and Kowalczykowski,S.C. (1992) Biochemical basis of the constitutive repressor cleavage activity of recA730 protein. A comparison to recA441 and recA803 proteins. *J. Biol. Chem.*, **267**, 20648–20658.
75. Bobst,E., Bobst,A., Perrino,F., Meyer,R. and Rein,D. (1985) Variability in the nucleic acid binding site size and the amount of single-stranded DNA-binding protein in Escherichia coli. *FEBS Lett.*, **181**, 133–137.
76. Li,G.-W., Burkhardt,D., Gross,C. and Weissman,J.S. (2014) Quantifying absolute protein synthesis rates reveals principles underlying allocation of cellular resources. *Cell*, **157**, 624–635.
77. Fisher,J.K., Bourniquel,A., Witz,G., Weiner,B., Prentiss,M. and Kleckner,N. (2013) Four-dimensional imaging of E. coli nucleoid organization and dynamics in living cells. *Cell*, **153**, 882–895.
78. Marceau,A.H., Bahng,S., Massoni,S.C., George,N.P., Sandler,S.J., Marians,K.J. and Keck,J.L. (2011) Structure of the SSB–DNA polymerase III interface and its role in DNA replication. *EMBO J.*, **30**, 4236–4247.
79. Fossum,S., Crooke,E. and Skarstad,K. (2007) Organization of sister origins and replisomes during multifork DNA replication in Escherichia coli. *EMBO J.*, **26**, 4514–4522.
80. Henrikus,S.S., Henry,C., Ghodke,H., Wood,E.A., Mbele,N., Saxena,R., Basu,U., van Oijen,A.M., Cox,M.M. and Robinson,A. (2019) RecFOR epistasis group: RecF and RecO have distinct localizations and functions in Escherichia coli. *Nucleic Acids Res.*, **47**, 2946–2965.
81. Lieberman,H.B. and Witkin,E.M. (1983) DNA degradation, UV sensitivity and SOS-mediated mutagenesis in strains of Escherichia coli deficient in single-strand DNA binding protein: effects of mutations and treatments that alter levels of exonuclease V or RecA protein. *Mol. Gen. Genet.*, **190**, 92–100.
82. Mount,D.W., Walker,A.C. and Kosel,C. (1975) *Molecular Mechanisms for Repair of DNA*. Springer, pp. 383–388.
83. Kowalczykowski,S.C., Dixon,D.A., Eggleston,A.K., Lauder,S.D. and Rehrauer,W.M. (1994) Biochemistry of homologous recombination in Escherichia coli. *Microbiol. Mol. Biol. Rev.*, **58**, 401–465.
84. Xia,J., Chiu,L.-Y., Nehring,R.B., Nunez,M.A.B., Mei,Q., Perez,M., Zhai,Y., Fitzgerald,D.M., Pribis,J.P. and Wang,Y. (2019) Bacteria-to-human protein networks reveal origins of endogenous DNA damage. *Cell*, **176**, 127–143.
85. Boeynaems,S., Alberti,S., Fawzi,N.L., Mittag,T., Polymenidou,M., Rousseau,F., Schymkowitz,J., Shorter,J., Wolozin,B. and Van Den Bosch,L. (2018) Protein phase separation: a new phase in cell biology. *Trends Cell Biol.*, **28**, 420–435.
86. Fleming,E., Yuan,A.H., Heller,D.M. and Hochschild,A. (2019) A bacteria-based genetic assay detects prion formation. *Proc. Natl Acad. Sci. U.S.A.*, **116**, 4605–4610.
87. Bianco,P.R. (2017) The tale of SSB. *Prog Biophy Mol Biol*, **127**, 111–118.
88. Crickard,J.B., Xue,C., Wang,W., Kwon,Y., Sung,P. and Greene,E.C. (2019) The RecQ helicase Sgs1 drives ATP-dependent disruption of Rad51 filaments. *Nucleic Acids Res.*, **47**, 4694–4706.